Geochemistry Geophysics Geosystems G3
AN ELECTRONIC JOURNAL OF THE EARTH SCIENCES
Published by AGU and the Geochemical Society

Article
Volume 6, Number 11
15 November 2005
Q11009, doi:10.1029/2005GC001026
ISSN: 1525-2027

Temporal and spatial variability in the composition of lavas exposed along the Western Blanco Transform Fault

Meagen A. Pollock, Emily M. Klein, and Jeffrey A. Karson
Division of Earth and Ocean Sciences, Duke University, 103 Old Chemistry Building, Box 90227, Durham, North Carolina 90277, USA (meagen.pollock@duke.edu)

Maurice A. Tivey
Department of Geology and Geophysics, Woods Hole Oceanographic Institution, 360 Woods Hole Road, Woods Hole, Massachusetts 02543, USA

[1] The northern scarp of the Western Blanco Transform (BT) Fault Zone provides a "tectonic window" into crust generated at an intermediate-rate spreading center, exposing a ~2000 m vertical section of lavas and dikes. The lava unit was sampled by submersible during the Blancovin dive program in 1995, recovering a total of 61 samples over vertical distances of ~1000 m and a lateral extent of ~13 km. Major element analyses of 40 whole rock samples exhibit typical tholeiitic fractionation trends of increasing FeO*, Na_2O, and TiO_2 and decreasing Al_2O_3 and CaO with decreasing MgO. The lava suite shows a considerable range in extent of crystallization, including primitive samples (Mg# 64) and evolved FeTi basalts (FeO > 12%; TiO_2 > 2%). On the basis of rare earth element and trace element data, all of the lavas are incompatible-element depleted normal mid-ocean ridge basalts (N-MORB; La/Sm_N < 1). The geochemical systematics suggest that the lavas were derived from a slightly heterogeneous mantle source, and crystallization occurred in a magmatic regime of relatively low magma flux and/or high cooling rate, consistent with magmatic processes occurring along the present-day southern Cleft Segment. The BT scarp reveals the oceanic crust in two-dimensional space, allowing us to explore temporal and spatial relationships in the horizontal and vertical directions. As a whole, the data do not appear to form regular spatial trends; rather, primitive lavas tend to cluster shallower and toward the center of the study area, while more evolved lavas are present deeper and toward the west and east. Considered within a model for construction of the upper crust, these findings suggest that the upper lavas along the BT scarp may have been emplaced off-axis, either by extensive off-axis flow or off-axis eruption, while the lower lavas represent axial flows that have subsided with time. A calculation based on an isochron model for construction of the upper crust suggests that the Cleft Segment requires at least ~50 kyr to build the lower extrusive section, consistent to first order with independent estimates for the construction of intermediate-spreading rate crust.

Components: 9974 words, 10 figures, 1 table.

Keywords: accretion; isochron; MORB.

Index Terms: 1032 Geochemistry: Mid-oceanic ridge processes (3614, 8416); 1065 Geochemistry: Major and trace element geochemistry; 3035 Marine Geology and Geophysics: Midocean ridge processes.

Received 20 May 2005; **Revised** 29 August 2005; **Accepted** 9 September 2005; **Published** 15 November 2005.

Pollock, M. A., E. M. Klein, J. A. Karson, and M. A. Tivey (2005), Temporal and spatial variability in the composition of lavas exposed along the Western Blanco Transform Fault, *Geochem. Geophys. Geosyst.*, *6*, Q11009, doi:10.1029/2005GC001026.

1. Introduction

[2] Our understanding of variations in magma composition at intermediate to fast-rate spreading centers has been based largely on studies of the lava carapace that caps the surface of the igneous ocean crust. Sampling of very young lavas along-axis demonstrates that sub-axial magmatic processes often generate magmas of similar compositions within distinct axial segments, while sampling along a flow line reveals the evolution of these processes over time [e.g., *Batiza et al.*, 1996; *Perfit and Chadwick*, 1998; *Regelous et al.*, 1999]. In each of these types of studies, it is assumed that the lavas sampled on the surface provide information on the axial processes that produce the crust of that age (i.e., near "zero-age" for along-axis samples; progressively older lavas along a flow line perpendicular to the axis). The existence of young off-axis volcanism [*Perfit et al.*, 1994; *Goldstein et al.*, 1994] or axial flows extending a few kilometers from the axis [*Perfit and Chadwick*, 1998; *Schouten et al.*, 1999; *Soule et al.*, 2005], however, clearly complicate this simple approach to studying variations in lava composition through time. In addition, studies of lavas from ophiolites and ODP drill cores reveal that the compositions of lavas within a lava pile may vary significantly with depth below the seafloor. Thus inferences based on surface sampling of off-axis lavas may provide an incomplete view of the true variability of magmatic processes occurring over a limited time span [*Perfit and Chadwick*, 1998].

[3] Ocean drilling and ophiolites provide valuable opportunities to investigate the variability of the ocean crust with depth, but each is limited in its applicability. While much has been learned about the structure and composition of the crust through ocean drilling [e.g., *Pariso and Johnson*, 1989; *Alt et al.*, 1996], by their nature these drill cores provide only a one-dimensional perspective on the ocean crust. Ophiolites, such as the Troodos ophiolite in Cyprus and the Semail ophiolite in Oman, provide accessible two- and three-dimensional exposures of oceanic lithosphere [e.g., *Moores and Vine*, 1971; *Pallister and Hopson*, 1981; *Nicolas*, 1989], but uncertainties regarding tectonic setting, spreading rate, and emplacement overprinting make ophiolites an imperfect analog for in situ ocean crust [*Moores and Vine*, 1971; *Dewey and Bird*, 1971; *Dilek et al.*, 2000; *Hawkins*, 2003].

[4] The study of tectonic windows into the oceanic crust presents an alternative and complement to both drilling and ophiolite studies. Tectonic windows occur at faulted escarpments where kilometer-scale vertical crustal sections of the oceanic crust are exposed. Tectonic windows into intermediate- to fast-spread crust are relatively rare and limited to propagating rifts and major transform faults. Direct observations of the structural, geochemical, and hydrothermal relationships offer insights into ocean crust accretion unmatched by other approaches, provided the effects of exposure mechanisms are recognized (see *Karson* [1998] for references and review). Studies of fast-spread crust exposed at the Hess Deep Rift, for example, suggest a 4-D model for accretion in which dikes transport magma along-axis and rapid sub-axial subsidence accommodates thickening of the lava unit [*Karson et al.*, 2002a; *Stewart et al.*, 2002].

[5] The north wall of the Western BT Fault Zone also represents a tectonic window, in this case exposing crust generated at an intermediate-rate spreading center. This study focuses on the spatial and temporal geochemical relationships among lavas exposed along a 13-km-long portion the BT scarp. These lavas provide information on the processes of crustal accretion that occurred over 400 kyr ~1 Myr ago at the southern end of the intermediate-spreading Cleft Segment of the Juan de Fuca Ridge. Through studies of tectonic windows like the BT, we hope to gain a better understanding the processes that lead to the development of the ocean crust through time.

2. Geologic Setting of the Blanco Transform

[6] The BT is a 360 km-long, left-lateral, dextrally slipping transform zone in the northeast Pacific (Figure 1) [*Embley and Wilson*, 1992; *Karson et al.*, 2002b]. It links the Cleft Segment of the Juan de Fuca Ridge (JdFR) in the north to the Gorda Ridge in the south. A pseudofault trace located about 60 km east of the current JdFR-BT intersection indicates previous southward propagation of the JdFR [*Juteau et al.*, 1995], terminating at the transform between 1.5 and 2 Myr ago [*Wilson et al.*, 1984]. Since then, the BT and Cleft Segment have been stable spreading features, separating the Juan de Fuca and Pacific plates. The western portion of the BT, located between the ridge-transform intersection (RTI) and the pseudofault, consists of a deep trough (~4800 mbsl) and a steep northern scarp (45°–50°). The north wall exposes just over 2 km of the upper oceanic crust, including the lava unit and upper portion of the dike unit

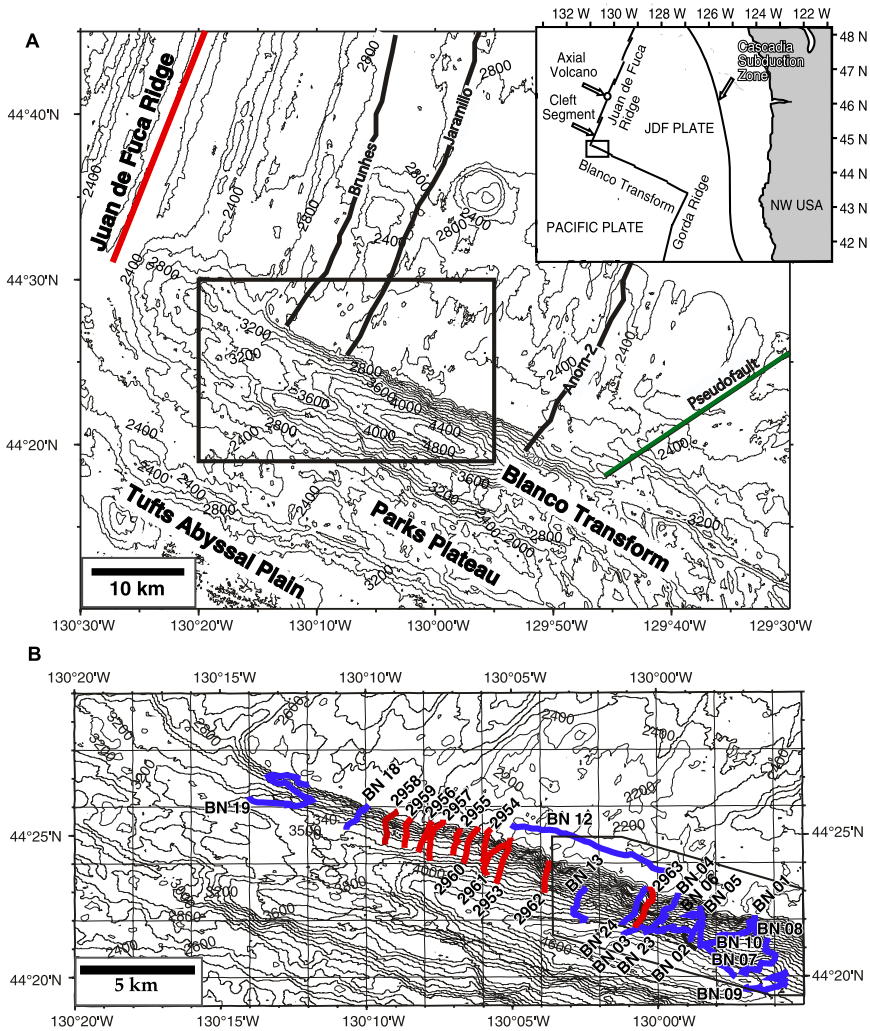

Figure 1. (a) Bathymetric map of the western Blanco Transform (100 m contour interval) with regional setting shown in inset. Box defines the boundaries of the study area enlarged in figure 1b. (b) Bathymetric map (50 m contour interval) of study area. *Alvin* dives from the Blancovin program, studied here, are shown in red (M. A. Tivey, unpublished data, 1995); *Blanconaute* (BN) dives, not studied here, are shown in blue [*Naidoo*, 1998; T. Juteau, unpublished data, 1991]. Side-scan sonar investigations are located within outlined box at right [*Delaney et al.*, 1987; *Naidoo*, 1998]. Bathymetric maps are modified after *Tivey* [1996]. Inset is modified from the National Oceanographic and Atmospheric Association's Pacific Marine Environmental Laboratory "Vents Program" Web site (http://www.pmel.noaa.gov/vents/).

[*Delaney et al.*, 1987; *Karson et al.*, 2002b]. Lavas exposed on the north wall of the BT were erupted along the southern Cleft Segment, which is spreading at an intermediate full rate of 60 mm/yr [*Delaney et al.*, 1981; *Riddihough*, 1984].

[7] Previous investigations include extensive sampling by submersible and dredging, geologic observations by side-scan sonar, deep sea and submersible photos, and detailed magnetic profiling of ~30 km of the north wall along the western Blanco scarp [*Delaney et al.*, 1987; *Juteau et al.*, 1995; *Tivey*, 1996; *Tivey et al.*, 1998; *Naidoo*, 1998; *Karson et al.*, 2002b]. The exposure consists mainly of an extrusive unit, ~900–1000 m thick, underlain by a sheeted dike complex (Figure 2) [*Juteau et al.*, 1995; *Karson et al.*, 2002b]. In general, the upper lavas are undeformed within the upper 200–500 m (exhibiting well-developed pillow and lobate morphologies with rare sheet flows) and grade downward into more fractured lavas. The lava flows dip toward the spreading center; the dip of lava flows increases with depth from an average dip of 23.8° in the upper lavas to

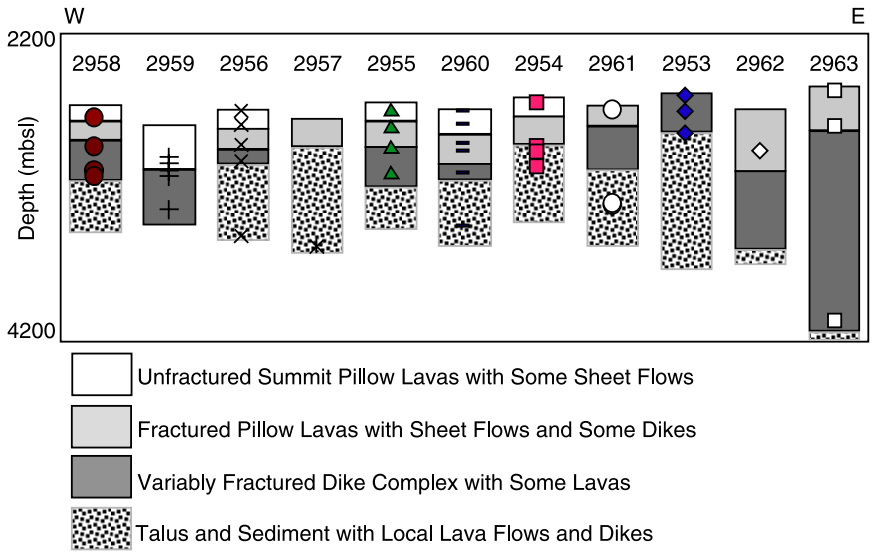

Figure 2. Schematic representation of the lithologies observed along the north wall of the BT during the Blancovin program. *Alvin* dive numbers are labeled at the top of the scarp. The dives are ordered across the exposure according to relative distance from the JdFR-BT intersection. Symbols indicate sample locations.

37.2° in the lower lavas [*Karson et al.*, 2002b]. Beneath the extrusive unit lies the sheeted dike complex, which is exposed for vertical intervals of as much as ~500 m before it is obscured by talus lower on the scarp. Dikes dip away from the spreading axis at angles typically between 40° and 50° [*Karson et al.*, 2002b]. Rare exposures of massive, possibly gabbroic rocks were observed beneath the sheeted dike unit [*Karson et al.*, 2002b].

[8] Additional information on the architecture of the upper ocean crust derives from studies of the magnetic reversal boundaries within the lava unit. In a study of the BT, *Tivey et al.* [1998] showed that magnetic reversal boundaries extend horizontally over ~3–4 km and systematically dip toward the spreading axis [*Tivey et al.*, 1998]. In the upper, undeformed lavas, the polarity boundaries dip at shallow angles (<5°), while in the lower lava section, the boundaries have a steeper dip (30°–45°).

3. Sampling and Sample Description

[9] This study focuses on the geochemistry of lavas collected during the 1995 Blancovin dive program to the north wall of the Blanco Transform between 130°04′W and 130°09′W (Figure 1). The dives are located between 24 and 37 km east of the intersection of the southern JdFR and the BT. Eleven *Alvin* dives, spaced approximately 1 km apart, recovered 61 samples from the extrusive unit, including 53 basalts and 8 breccias (Figure 2). Each dive traversed ~2000 m of vertical exposure and collected an average of 5 samples. Assuming a constant half-spreading rate of 30 mm/yr for the JdFR [*Delaney et al.*, 1981; *Riddihough*, 1984], the sample suite spans from 0.8 to 1.2 Myr in age and represents ~400 kyr of accretion.

[10] The lavas range in morphology from sheet flows to pillow lavas. Brown alteration rinds penetrate the outer ~1 cm of most of the samples. Millimeter-scale glass rims border some of the lavas. Thin-section observations show that the lavas are aphyric to weakly porphyritic, ranging from 1–9% (by volume) phenocrysts, although most have <3%. Plagioclase is the dominant phenocryst phase and exists as euhedral laths (<1 mm long) or as glomerocrysts in a fine-grained or glassy matrix. Some larger plagioclase grains enclose smaller laths while other large plagioclase crystals show partial resorption textures. Phenocrysts of clinopyroxene occur in some of the more evolved samples while microphenocrysts of olivine are present in some of the primitive samples. Across the range of basalt compositions, the variolitic groundmass consists of clinopyroxene and plagioclase with less abundant opaque oxides and glass. Many of the samples are finely (<1 mm) vesicular (0–10% vesicles).

[11] All of the samples are altered to various extents, as demonstrated by brown alteration rinds and mineral alteration products. Visibly altered

material was avoided during sample preparation by selecting samples with fresh gray interiors and by excluding alteration halos. Of the 53 basalts recovered, 40 samples appeared sufficiently fresh for chemical analysis. Some obviously altered samples (2962-1, 2962-2, 2963-5, 2963-6) were analyzed for comparison, but are excluded from the interpretations. Comparison of the fresh and altered samples reveals the effects of low-temperature seawater alteration (i.e., secondary chlorite and epidote). The altered samples show high (>1.5%) loss on ignition (LOI), a good indicator of alteration by seawater [*Alt*, 1993]. All of the lavas that are considered fresh have LOI <1.5%. Generally, the fresh interiors appear unaltered; however the elements K, Rb, Ba, and Sr may have been mobilized by seawater reactions, as evidenced by their high variability (K, Rb, and Ba concentrations vary more than 100% while Sr abundances vary by ~60%). These elements are excluded from further interpretation.

4. Analytical Methods

[12] Major and trace element analyses were performed at Duke University on whole rock powders prepared with an agate mortar and pestle. Major elements (in a 1:4750 dilution) and high-abundance trace elements (in a 1:250 dilution) were measured by direct current plasma emission spectrometry (DCP; Fisons SpecterSpan 7) using a procedure modified after *Klein et al.* [1991]. The standards used for calibration of DCP data were NBS-688, AII92-29-1, and K1919 (similar to BHVO-1). Low-abundance trace element concentrations were analyzed by inductively coupled plasma mass spectroscopy (ICP-MS; VG-Elemental PlasmaQuad 3) using a procedure modified after *Cheatham et al.* [1993]. The standards used for calibration in the ICP-MS analyses were U.S. Geological Survey standards: BHVO-1, BIR-1, DNC, and W2-1. Each run consisted of repeat analyses of samples (duplicate for DCP runs and triplicate for ICP runs), standards, blank, and a solution to monitor machine drift. Additionally, some samples were prepared in duplicate and analyzed in separate runs.

5. Results

5.1. Major Elements

[13] The abundance of major and trace elements in the BT lavas are presented in Table 1. Unlike glasses, which may be assumed to be equivalent to liquid compositions, whole rock analyses represent melt plus crystals. Generally, the effects of crystal accumulation on the BT lavas appear to be minimal. Plagioclase is the dominant phenocryst phase in the BT lavas, but the effects of plagioclase accumulation (i.e., systematic changes in MgO, FeO*, CaO, Al_2O_3) are only observed in a small number of samples (2958-2, 2956-2). In contrast, evidence of plagioclase fractionation is expressed throughout the BT suite by negative Eu anomalies (Figure 4). Elevated abundances of Ni (2958-1, 2956-6) and Sc (2961-4) in a small number of samples also suggest minor accumulation of olivine and clinopyroxene, interpretations corroborated by thin section and hand sample observations.

[14] Compared to the global range in major element compositions, the compositions of the BT lavas generally overlap with and span the variability observed among MORB from the northern EPR (Figure 3) [*Klein and Langmuir*, 1987; *Klein et al.*, 1991]. The BT samples exhibit substantial overlap with axial and off-axis lavas specifically from the southern JdFR (M. Perfit, personal communication), with an average MgO concentration of 6.9 ± 0.9 wt% and an average of 11.5 ± 1.5 wt% FeO*. The BT lavas have Mg# values of 65-40, representing relatively primitive to moderately evolved samples [*Hess*, 1989]. Major element variations display typical low-pressure (1 kb) crystallization trends for a tholeiitic magma of increasing FeO*, TiO_2, and Na_2O and decreasing Al_2O_3 and CaO with decreasing MgO. Eleven of the samples, classified as FeTi basalts (FeO* >12%, TiO_2 >2% [*Byerly*, 1980]), are among the most evolved in the suite with Mg#s less than 48.

[15] Liquid lines of descent (LLDs) were calculated, using the program of *Weaver and Langmuir* [1990] and primitive BT sample 2955-8 as the parent composition (MgO ~9.0 wt%, Mg# 63; Figure 3). The successive crystallization and fractionation of olivine, followed by olivine + plagioclase, then olivine + plagioclase + clinopyroxene from the assumed parent magma produces a characteristic tholeiitic differentiation trend for the BT major element data, which are best described by up to 60% crystallization. To first-order, the 1-kb fractional crystallization LLD approximates most of the data; however, at a constant value of MgO, the samples show variability in other oxides that cannot be reproduced by variations in the pressure of crystallization, suggesting that fractional crystallization of a single parent is not the sole process

Table 1 (Representative Sample). Major and Trace Element Data for Whole Rock Samples From the Blanco Transform[a] [The full Table 1 is available in the HTML version of this article at http://www.g-cubed.org]

Sample ID	2953-3	2953-5	2953-6	2954-4	2954-5	2954-6	2954-7	2954-8	2955-2	2955-3	2955-7	2955-8	2956-1	2956-2	2956-3	2956-5	2956-6	2957-1	2958-1	2958-2
Depth, m	2679	2456	2336	3039	2896	2877	2877	2412	3053	2881	2644	2494	3645	2932	2797	2581	2498	3784	2956	2949
Latitiude	44.409	44.411	44.413	44.409	44.411	44.412	44.412	44.421	44.416	44.417	44.419	44.421	44.408	44.420	44.421	44.424	44.427	44.403	44.425	44.426
Longitude	130.086	130.085	130.084	130.099	130.099	130.098	130.098	130.094	130.115	130.114	130.113	130.112	130.136	130.131	130.131	130.129	130.129	130.130	130.155	130.155
Dist. from axis, km	32.95	33.00	33.07	31.90	31.90	31.94	31.94	32.32	30.64	30.73	30.78	30.82	28.92	29.33	29.38	29.50	29.52	29.40	27.42	27.42
SiO_2, wt%	51.41	50.40	49.61	50.49	49.69	50.07	49.64	49.83	50.05	50.30	49.98	48.77	50.18	50.21	49.40	49.93	50.27	49.53	49.51	49.87
TiO_2	2.48	1.74	1.69	1.62	2.86	1.95	1.96	1.49	2.18	2.04	1.40	1.19	2.05	2.43	2.62	1.49	2.68	1.85	2.43	2.94
Al_2O_3	14.21	14.47	13.92	14.85	12.62	13.80	14.25	14.29	13.94	13.90	15.13	16.17	14.00	14.07	13.69	14.03	13.15	13.88	13.20	13.09
Fe_2O_3	12.72	11.90	12.72	11.01	16.36	13.23	13.07	10.88	13.36	12.69	10.75	10.10	12.88	13.79	14.55	11.83	14.24	12.96	14.58	15.63
FeO*	11.45	10.71	11.45	9.91	14.72	11.90	11.76	9.79	12.02	11.42	9.67	9.09	11.59	12.41	13.09	10.65	12.81	11.66	13.12	14.07
MnO	0.22	0.19	0.20	0.19	0.24	0.21	0.19	0.23	0.21	0.21	0.18	0.17	0.21	0.20	0.22	0.21	0.22	0.21	0.21	0.21
MgO	5.89	7.16	8.11	7.05	5.96	6.77	6.58	7.68	6.20	6.68	7.32	8.82	6.67	5.93	5.95	7.85	6.33	7.08	6.67	5.79
CaO	11.19	12.44	11.28	13.19	10.09	11.46	11.33	12.50	11.35	11.52	12.15	12.40	11.70	10.72	10.74	12.51	10.07	11.31	10.53	9.82
Na_2O	2.83	2.56	2.57	2.76	2.75	2.66	2.77	2.57	2.63	2.48	2.34	2.20	2.66	2.74	2.92	2.53	2.83	2.48	2.61	2.76
K_2O	0.35	0.08	0.16	0.13	0.28	0.14	0.11	0.16	0.23	0.21	0.17	0.15	0.24	0.25	0.36	0.44	0.35	0.30	0.28	0.17
Total	101.30	100.95	100.26	101.29	100.83	100.29	99.89	99.61	100.15	100.02	99.42	99.97	100.59	100.35	100.46	100.82	100.14	99.60	100.02	100.29
Mg#	47.9	54.4	55.8	55.9	41.9	50.3	49.9	58.3	47.9	51.1	57.4	63.3	50.6	46.0	44.8	56.8	46.8	52.0	47.5	42.3
LOI	0.7	0.1	0.7	0.8	1.1	1.3	1.1	0.5	1.1	0.6	0.3	0.0	0.0	0.3	0.2	0.9	0.2	0.3	0.5	0.7
Sr, ppm	124	108	106	131	107	104	108	123	103	90	100	108	112	113	115	103	101	112	112	106
Ba	26.27	10.41	10.26	15.06	16.84	11.67	11.85	18.31	13.92	13.98	10.28	10.64	15.31	13.34	28.01	33.81	43.28	16.84	19.68	11.45
Zn	127	140	93	82	137	101	102	87	116	101	81	72	101	98	120	152	137	98	100	81
Cu	59	76	62	63	54	57	68	70	59	55	60	71	62	62	59	52	50	64	59	54
Ni	88	98	91	95	65	84	88	102	105	92	93	121	84	88	67	137	114	86	129	87
V	441	355	336	351	524	409	389	331	437	420	335	275	374	388	404	506	494	368	405	343
Sc	46.1	45.3	43.8	46.3	45.6	46.0	43.9	47.9	46.4	44.3	42.6	37.2	44.9	44.4	44.2	40.1	41.8	45.1	44.0	46.3
Cr	126	203	146	251	60	157	143	301	169	225	262	310	174	240	95	204	214	184	144	183
P	1252	606	810	664	1319	947	972	714	928	946	686	531	925	860	1214	1615	1589	999	886	634
Y	58	32	40	35	66	46	44	34	53	48	35	28	46	41	66	76	73	46	46	34
Zr	175	98	117	99	192	130	127	99	165	145	111	85	146	116	234	225	233	171	122	97
Be	1.40	0.83	0.75	0.74	2.95	1.06	1.01	0.83	3.01	0.99	0.73	0.63	1.05	1.01	1.55	1.67	1.67	1.16	1.06	0.75
Co	52.5	43.1	46.7	42.0	46.8	44.6	46.9	42.9	48.1	44.7	40.0	44.1	45.4	43.7	45.1	59.4	45.5	45.2	52.2	42.3
Ga	16.5	13.7	13.4	13.4	16.4	14.1	14.4	13.0	15.0	14.1	13.1	12.2	14.0	13.6	16.4	17.1	17.9	13.9	14.6	12.4
Rb	3.65	0.79	2.17	1.48	1.94	1.83	1.09	1.84	2.58	2.04	2.37	1.30	1.68	2.34	4.69	9.26	3.32	2.65	2.81	0.72
Nb	6.63	2.97	3.18	3.45	6.18	3.86	3.81	3.33	4.52	4.07	2.85	2.42	4.71	4.21	6.22	7.55	7.37	4.64	3.88	3.10
Cs	0.073	0.016	0.016	0.055	0.015	0.015	0.038	0.016	0.049	0.055	0.046	0.021	0.019	0.060	0.070	0.407	0.038	0.018	0.092	0.009
La	6.38	2.86	3.45	3.46	6.36	4.17	4.04	3.48	4.65	4.28	3.17	2.57	4.78	4.27	7.31	7.97	7.61	4.69	3.99	3.12

[a] Major element oxides are reported in weight%; trace elements in ppm. FeO* is total Fe recalculated as FeO. Mg# is calculated as cation mole% [Mg/(Mg+Fe)]. Major elements and Sr, Sc, Zn, and V were analyzed by DCP. Reproducibility for DCP analyses is 1-2% for all major and minor elements with the exception of the following: <4% for Zn; <3% for Sc and V. The remaining trace elements were analyzed by ICP-MS, for which the reproducibility is 1–3% for REE and 1–5% for all other elements. Replicate analyses of standards are in agreement with previously published values (see electronic database of *Stewart et al.* [2002]).

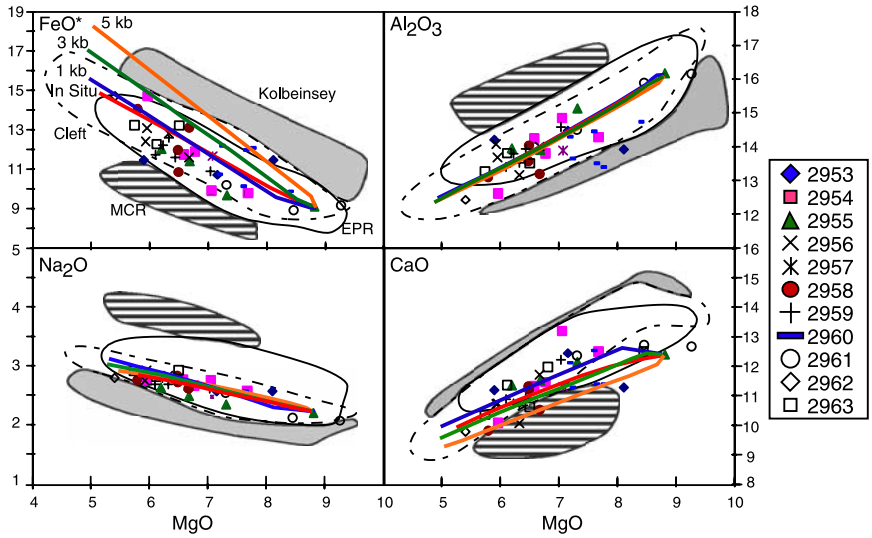

Figure 3. Major element variations for the Blanco Transform samples. Clockwise from top left: FeO*, Al_2O_3, CaO, and Na_2O versus MgO (wt%). The samples are identified by dive as in Figure 2. Symbols are larger than analytical error ($\pm 1\sigma$). Fields show global range in N-MORB compositions from the Kolbeinsey Ridge (gray), Mid-Cayman Rise (MCR; horizontal stripe), and northern East Pacific Rise (EPR; unshaded). MORB from the Cleft Segment (dashed line) overlap with the northern EPR field. Data for the Kolbeinsey Ridge, MCR, and EPR are from the Ridge Petrological Database of the Ocean Floor (http://www.petdb.org/index.jsp). Data from the Cleft Segment are from PetDB and M. Perfit (personal communication) and include both on- and off-axis samples, which extend the Cleft Segment field to more evolved compositions. Liquid lines of descent (LLDs) are calculated using the program of *Weaver and Langmuir* [1990] for 1-kb (blue), 3-kb (green), and 5-kb (orange) fractional crystallization. The data are best described by up to 60% crystallization at ~1 kb with final proportions of plag:ol:cpx of approximately 50:14:36. The LLD produced by in situ crystallization (red) is also shown. The in situ curve is calculated using the methods of *Reynolds and Langmuir* [1997] and *Stewart et al.* [2002]. All models are calculated under anhydrous conditions. The primitive BT sample 2955-8 is used as a parental composition. This composition is not considered primary but may be a parental melt candidate as it is one of the most primitive compositions sampled in the BT suite. The more magnesian samples 2961-2 and 2961-3 were modeled but provided poor fits to the data because of low Na_2O concentrations.

affecting this suite of lavas. Lavas collected from the axis of the Cleft Segment exhibit similar trends in crystallization [*Smith et al.*, 1994].

5.2. Trace Elements

[16] On the basis of REE data, all of the lavas recovered along the north wall of the Blanco scarp are normal MORB (N-MORB) [*Sun and McDonough*, 1989] (Figure 4). The BT lavas are depleted in the highly incompatible elements and light rare earth element (La/Sm_N of 0.65 ± 0.06), but show relatively flat trends in the moderately incompatible elements (e.g., Zr/Y of 1.22 ± 0.11), patterns similar to those of axial lavas from the Cleft Segment [*Smith et al.*, 1994]. REE abundances normalized to chondritic values [*Sun and McDonough*, 1989] reveal patterns that are consistent with the effects of fractional crystallization (Figure 4). In general, more evolved lavas with low Mg# have higher abundances of REE and more negative Eu anomalies.

[17] Incompatible trace element abundances plotted versus MgO also exhibit the effects of low-pressure (1 kb) fractional crystallization (Figure 5). However, the data show enrichments in incompatible elements with increasing fractionation that cannot be explained by simple crystal fractionation alone. Complex crystallization models, such as in situ crystallization, have been invoked to explain similar large enrichments in incompatible elements [*Langmuir*, 1989]. In this process, crystallization occurs within a boundary layer, creating an evolved liquid that is incorporated into the remaining less evolved melt in the magma chamber. The net effect of in situ crystallization is to enrich incompatible elements in the magma chamber to a greater extent than predicted by simple Rayleigh fractionation.

[18] The iterative methods of *Reynolds and Langmuir* [1997] and *Stewart et al.* [2002] were used to model the effects of in situ crystallization (Figure 5). The LLD produced by in situ crystal-

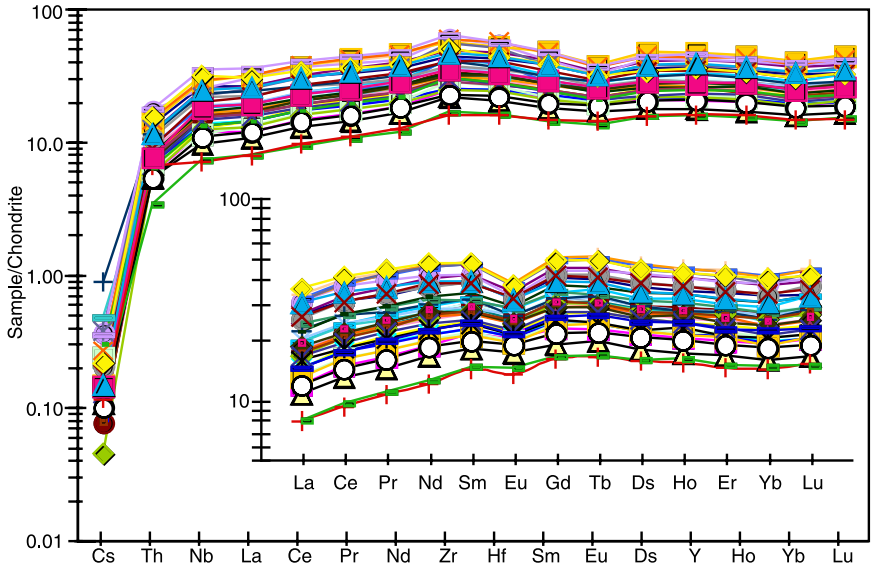

Figure 4. Chondrite-normalized trace element abundances [*Sun and McDonough*, 1989] in order of increasing compatibility for the BT lavas. Inset shows chondrite-normalized rare earth elements (REE). All of the BT lavas are incompatible-element depleted N-MORB ($La/Sm_N < 1$). The REE trends are consistent with the effects of fractional crystallization, with increasing abundances of REE and more negative Eu anomalies in the more evolved samples.

lization results in enrichments in incompatible trace elements that are more consistent with the observed data. On the basis of this crystallization model, the compositions of the most evolved samples are best described by 70% crystallization in a system with a boundary layer that constitutes 5% of the melt lens in which 35% crystallization occurs. Sample compositions that vary between the LLDs may be the result of mixing of melts affected by the two different crystallization processes [*Dixon et al.*, 1986; *Smith et al.*, 1994].

[19] While coupled fractional and in situ crystallization capture the bulk of the compositional diversity of the BT lavas, the samples also exhibit small but systematic variability in the ratios of various incompatible trace elements. Ratios of elements with similar incompatibilities (e.g., La/Sm_N, Zr/Y) are relatively insensitive to realistic amounts of crystallization (<70% crystallization [*Gast*, 1968]) and are only slightly modified by melting [*Shaw*, 1970; *Minster and Allegre*, 1978]. Thus the correlated variability in these ratios (e.g., Zr/Y from 2.5 to 3.7; La/Sm_N from 0.54 to 0.79)) suggests that the BT lavas have likely experienced some mixing of melts derived from a heterogeneous mantle source. This finding is also consistent with data for axial lavas collected from the Cleft Segment [*Smith et al.*, 1994].

5.3. Comparison of Blanco Transform Lavas to Lavas Erupted Along the Cleft Segment

[20] The similarity in major and trace element compositions between the ~1 Myr lavas exposed within the BT and near zero-age lavas sampled at the surface along the southern Cleft Segment suggests that petrogenetic conditions along the Cleft Segment have remained relatively stable over the past ~1 Myr (Figure 3). In particular, both suites are dominated by the effects of fractional crystallization and appear to have experienced a similar range of crystallization at shallow depths (~1 kb) [*Dixon et al.*, 1986; *Smith et al.*, 1994; *Tierney*, 2003; D. S. Stakes et al., The cleft revealed: Geologic, magnetic, and morphologic evidence for construction of upper oceanic crust along the southern Juan de Fuca Ridge, submitted to *Geochemistry, Geophysics, Geosystems*, 2005 (hereinafter referred to as Stakes et al., submitted manuscript, 2005)].

[21] Indeed, most of the previous geochemical work along the Cleft Segment has focused on the substantial and spatially systematic trend in the extent of low-pressure crystallization (Figure 6) [*Dixon et al.*, 1986; *Smith et al.*, 1994; *Tierney*, 2003; Stakes et al., submitted manuscript, 2005]. Lavas from the northern Cleft region (north of

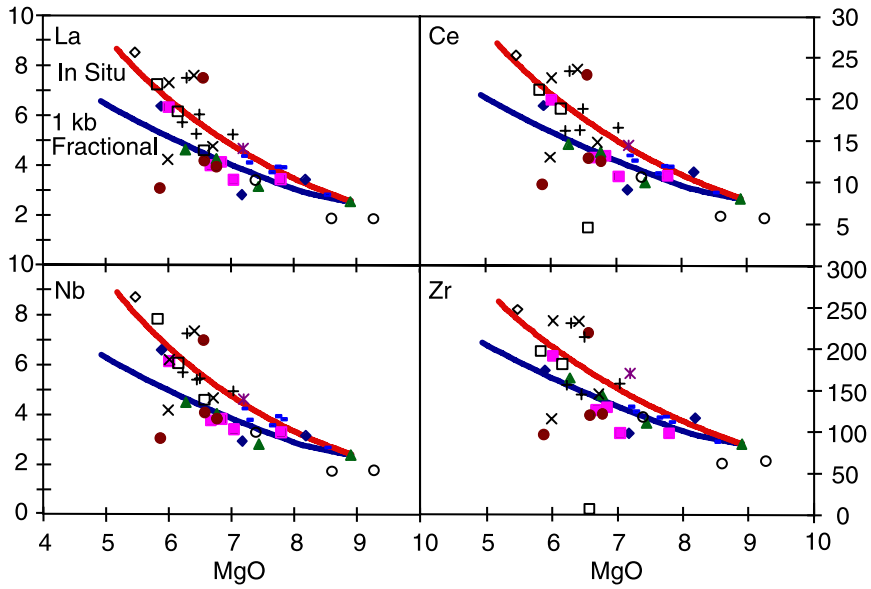

Figure 5. Selected trace element concentrations for the BT lavas. Clockwise from top left: La, Ce, Zr, and Nb (ppm) versus MgO (wt%). Symbols as in Figure 3. Symbols are larger than the analytical error (±1σ). The liquid line of descent produced by in situ crystallization is shown in red; the blue line indicates 1-kb fractional crystallization. Partition coefficients used in the calculation are from *Bedard* [1994]. The data are best described by 70% crystallization in a system with a boundary layer that constitutes 5% of the melt body and in which 35% crystallization occurs.

44°41′N; >25 km from the RTI) are largely primitive and restricted to a relatively narrow range in extent of fractionation (Mg# 50–62), suggesting a steady state magmatic system with sufficient melt supply to prevent magmas from cooling to great extents [*Smith et al.*, 1994]. Lavas from the southern Cleft Segment, however, are more diverse (Mg# 35–60) and evolved, reaching maximum extents of fractionation in the RTI where dacitic lavas were recovered [*Smith et al.*, 1994; *Cotsonika et al.*, 2005; Stakes et al., submitted manuscript, 2005]. The greater range in fractionation among the southern Cleft lavas suggests that low magma flux and/or greater cooling rates, possibly resulting from proximity to the RTI [*Fornari et al.*, 1983; *Perfit et al.*, 1983; *Sinton et al.*, 1983], lead to the existence of discrete, temporally and spatially evolving sub-axial magma bodies [*Smith et al.*, 1994; J. Canales et al., Upper crustal structure and axial topography at intermediate-spreading ridges: Seismic constraints from the Southern Juan de Fuca Ridge, submitted to *Journal of Geophysical Research*, 2005 (hereinafter referred to as Canales et al., submitted manuscript, 2005)]. The overall similarity between the lava compositions from the BT and those from the southern Cleft Segment, including their wide ranges in fractionation (Mg#s of ~35–65), suggests that the BT lavas formed in a regime of low magma flux and/or high cooling rate similar to that beneath the present axis of the adjacent southern Cleft Segment.

6. Discussion

6.1. Construction of the Upper Crust: Temporal and Spatial Relationships Along the BT Scarp

[22] To explore the spatial and temporal relationships among the lavas exposed along the BT, it is important to understand how the upper crust is constructed. The complexity of this is illustrated by the fact that even the deepest lavas exposed along the scarp originally erupted on the seafloor and must have subsided during spreading. Thus the upper crust is constructed by a combination of horizontal transport during seafloor spreading and vertical transport due to subsidence. Useful insights into these processes can be derived from geophysical and geological studies of the BT and other tectonic windows.

[23] Magnetic structures and geologic observations along the BT scarp (and other tectonic windows) suggest a model for crustal evolution in which the crust generated at the southern JdFR experiences rapid subsidence near the axis (within ~1–3 km) shortly after formation (Figure 7) [*Tivey*, 1996;

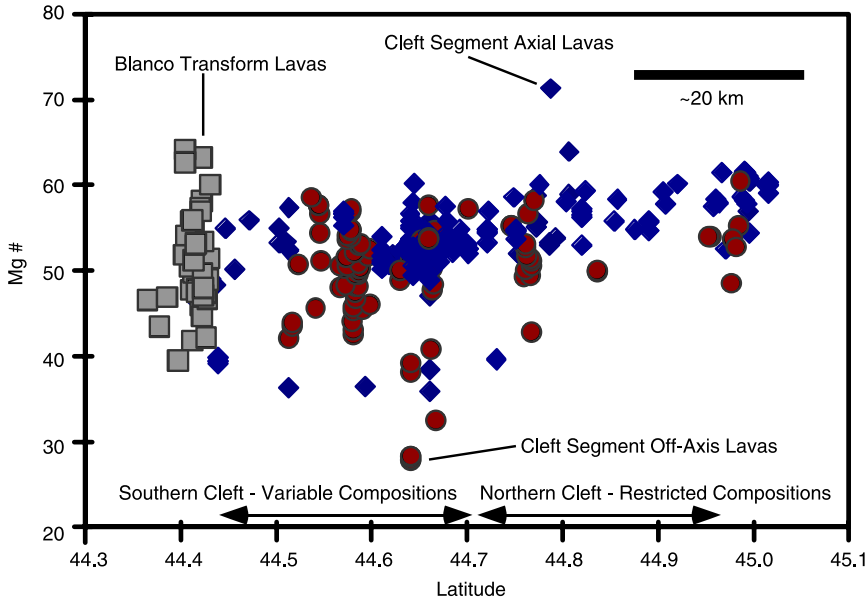

Figure 6. Basalt Mg# versus latitude for axial and off-axis lavas collected along the Cleft Segment and lavas from the BT. Cleft Segment data (blue diamonds represent on-axis samples; red circles represent off-axis samples) are from *Dixon et al.* [1986], *Smith et al.* [1994], *Tierney* [2003], and M. Perfit (personal communication). BT lavas (gray squares) are data from this study. On average, the Cleft Segment samples show a southward decrease in Mg#; while relatively primitive lavas are erupted along the length of the segment, the maximum extent of fractionation increases southward. Lavas become more diverse ~23 km north of the RTI, extending to highly evolved compositions toward the RTI (Stakes et al., submitted manuscript, 2005). This break in lava diversity divides the Cleft Segment into two distinct magmatic sections, the northern and the southern Cleft segments. Data from the BT overlap much of the range defined by the southern Cleft Segment lavas.

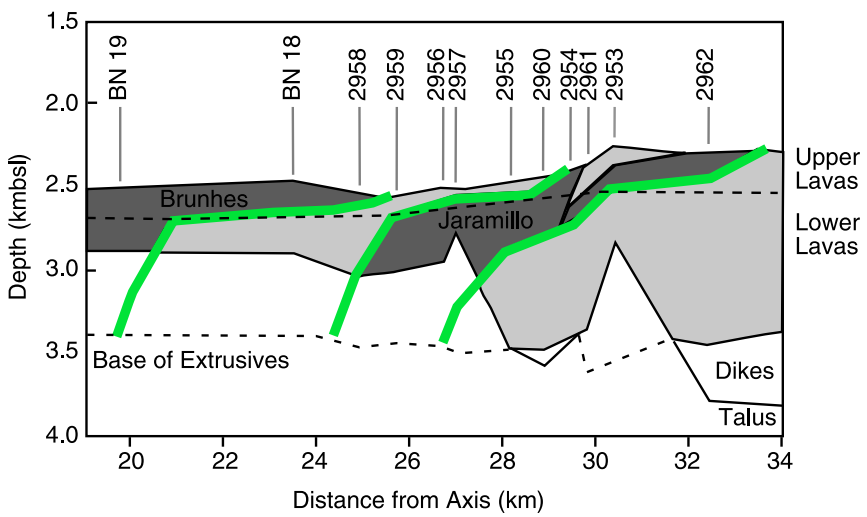

Figure 7. Schematic cross section of the Blanco scarp (modified after *Tivey et al.* [1998]). Green lines depict isochrons, which are determined from boundaries between lavas with opposite magnetization polarities (light field, normal polarity; dark field, reverse polarity). The dotted black lines show the boundaries between lithologic units (division between upper and lower lavas; and between lavas and dikes). *Alvin* dive locations are shown by vertical gray lines labeled with dive number.

Tivey et al., 1998; *Karson et al.*, 2002b]. As a result, the lava flows erupted on-axis tend to tilt toward the spreading center. As lateral spreading proceeds, axial lavas subside to greater depths, forming the base of the extrusive section, and flows dip toward the axis at increasingly steeper angles. Lavas can also be emplaced farther from the axis by voluminous flows that are channeled away from the axis or erupted beyond the axial valley [e.g., *Hooft et al.*, 1996; *Perfit and Chadwick*, 1998; *Soule et al.*, 2005]. Such lavas, because they are removed from the region of greatest subsidence (i.e., the ridge axis), will experience less subsidence than axial lavas and will dip toward the axis at a shallower angle. The result is a vertical sequence of lavas in which the lava flows dip toward the spreading center and the dips increase with depth. In terms of time variability in the upper crust, isochrons delineating lava flows of near-equal age would be expected to follow similarly curved paths that dip toward the spreading center.

[24] This model for construction of the extrusive unit of the ocean crust, which takes into account not only seafloor spreading (horizontal transport away from the axis) but also crustal subsidence (vertical transport downward), has important implications for both the spatial and temporal relationships among lavas exposed along the BT. With respect to spatial relationships, the model asserts that the base of the extrusive section is formed by lavas erupted on-axis and subsequently buried. In contrast, the upper lavas, which cap the extrusive unit, represent a combination of axially erupted lavas, voluminous off-axis flows, and lavas erupted off-axis through the crust. This suggests that flow line studies, which of necessity sample the upper lava carapace, may represent a biased sampling of the true diversity of magma compositions because they preferentially sample flows that are emplaced farther from the axis, while axial lavas, which form the base of the extrusive section, are more likely to be buried. In this sense, the lavas exposed along the BT should provide a more representative sampling of the diversity of magmas that form the crust.

[25] In regard to temporal relationships, as noted above, isochrons representing lavas of approximately equal age form curved trends that dip toward the spreading center. Thus, in order to examine chemical variations in lava composition through time, the most useful traverse to explore is one that trends perpendicular to the isochrons (because this represents both the most rapid changes in time with distance, and a succession of superimposed lavas). This time sequence trends diagonally through the crust, dipping away from the axis, with oldest lavas deepest and farthest from the axis and youngest lavas, of course, at the surface on-axis. While it is true that a vertical section through the upper ocean crust, such as a drill core, also represents increasing age with depth, according to the model described above, each overlying lava was emplaced further off-axis than the one below it, an effect that is minimized for traverses that are perpendicular to isochrons.

6.2. Comparison of Temporal and Spatial Variations in the Cleft Segment and BT Lavas

[26] Samples recovered from the southern Cleft Segment are surface lavas, which are commonly assumed to reflect recent magmatic conditions. Similarly, surface lavas sampled along a flow line extending away from the axis are assumed to reflect changing (or unchanging) conditions in the magma reservoir system beneath the ridge through time [e.g., *Batiza et al.*, 1996; *Regelous et al.*, 1999]. Although this simple view of crustal accretion may be complicated by off-axis volcanism or along-axis diking [e.g., *Perfit et al.*, 1994; *Stewart et al.*, 2003], studies of samples collected along flow lines elsewhere have revealed systematic changes in the composition of lavas. These chemical patterns are often symmetrical about the axis, consistent with a temporally evolving magma reservoir system beneath a given axial location [e.g., *Batiza et al.*, 1996].

[27] Previous investigations along the Cleft Segment have produced an extensive suite of axial and off-axis lavas, including samples collected along approximate flow lines extending both east and west of the axis [*Smith et al.*, 1994; *Tierney*, 2003; Stakes et al., submitted manuscript, 2005]. Spatial analysis of data for the entire Cleft Segment shows that the lavas sampled off-axis are generally more evolved than those recovered from the axis [*Tierney*, 2003; Stakes et al., submitted manuscript, 2005]. This spatial distribution of evolved and primitive lavas can be interpreted as reflecting a change in sub-axial magmatic conditions over time [*Reynolds et al.*, 1992; *Batiza et al.*, 1996], in which the older, more evolved lavas were erupted under conditions of waning magmatic activity while the younger, primitive lavas were erupted during more robust magmatism.

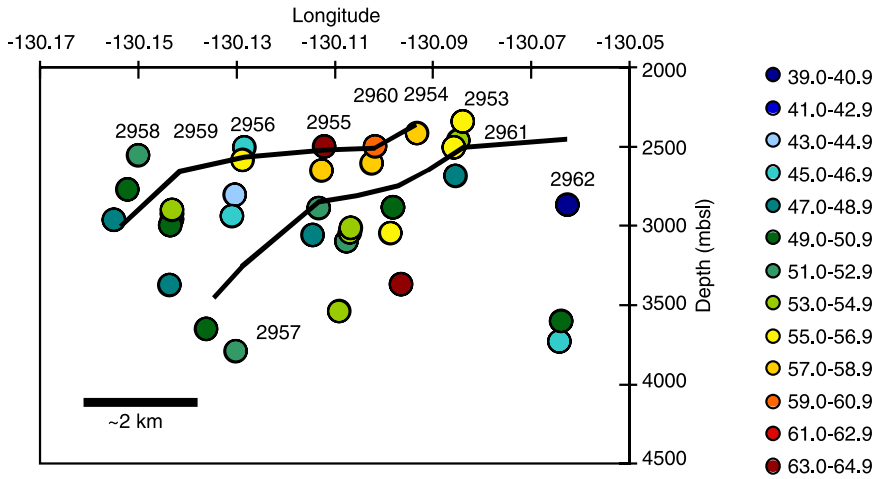

Figure 8. Longitude (°W) versus depth (m) for Blancovin samples located within area shown in Figure 7. Samples are color-coded by Mg#; blue samples are the most evolved in the suite (Mg# 39.0–40.9); red samples are the most primitive (Mg# 53.0–54.9). Solid black lines indicate magnetic isochrons from *Tivey et al.* [1998] and Figure 7. Dive numbers are indicated near the end of each dive with the exception of dive 2957, which only includes 1 sample analyzed here, and dive 2963, which is located ~5 km outside of the area shown. Primitive samples tend to cluster at shallow depths in the central portion of the study area, while more evolved samples predominate at depth and toward the east and west.

[28] An examination of the flow line traverses for the southern Cleft Segment, however, reveal complex relationships that cannot be easily explained by temporal evolution (Stakes et al., submitted manuscript, 2005). For example, two flow lines extending to the east show a general decrease in Mg# with distance from the spreading center, but one flow line resets to higher values of Mg# within 2 km of the axis. In contrast, a flow line extending to the west shows an increase in Mg# with distance from the axis. If indeed the flow line data represent an age-sequence, where age increases with distance from the axis, they demonstrate that separate portions of the southern Cleft Segment experience differing evolutionary histories.

[29] The BT scarp, which exposes the upper crust along an approximate flow line, allows us to explore evidence of the temporal evolution of the southern Cleft Segment ~1 Myr ago. Figure 8 shows the magnetic isochrons along the BT scarp as well as spatial variations in Mg# for the BT lavas. As a whole, the data are spatially variable and do not appear to form regular trends, apart from the finding that relatively primitive lavas tend to cluster shallower and toward the center, while more evolved lavas cluster deeper and toward the west and east.

[30] Recall that the model for crustal construction predicts that lavas representing age progressions should lie along sections perpendicular to the isochrons. On the basis of our present sampling of the BT, no systematic temporal changes are observed. While this is disappointing, it is perhaps not surprising for a number of reasons. First, our sample coverage is quite sparse, averaging ~2 samples/km^2. In addition, the only significant form of chemical variability in this data set is one of fractionation, and individual lava flows in other areas are known to display significant chemical variations across small spatial scales, particularly with respect to fractionation [*Perfit et al.*, 1994; *Sinton et al.*, 2002]. Lastly, in the absence of detailed age dating of the lavas, it is not known to what extent the lava carapace has been capped by off-axis eruptions, complicating the assumption of simple superposition of successive lavas.

[31] Indeed, Stakes et al. (submitted manuscript, 2005) argue that the evolved, off-axis lavas sampled along the Cleft Segment represent flank eruptions that tap the cooler, more fractionated edges of the magma chamber and periodically cap the more primitive axial lavas. Furthermore, they suggest that the upper lavas exposed in the BT scarp are analogous to the off-axis lavas sampled along the Cleft Segment. This idea can be explored in the context of the model for crustal construction developed above.

[32] The model for crustal construction asserts that lavas erupted on-axis experience more subsidence than lavas emplaced farther from the axis. Thus the

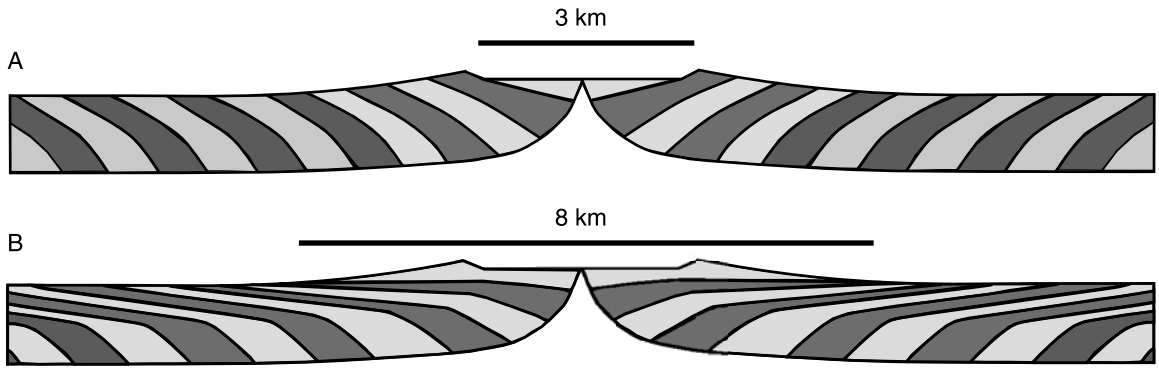

Figure 9. Schematic cross sections of the extrusive section accreting at a mid-ocean ridge. Alternating dark gray and light gray bands indicate constructional packets of lavas, separated by isochrons (solid black lines). (a) Crustal modeling assuming volcanic construction occurs entirely within a 3-km-wide neovolcanic zone. Axial lavas subside to form the base of the extrusive section, rotating toward the axis. Lavas emplaced farther from the axis near the axial valley wall still experience subsidence, but are rotated to a lesser degree. The resultant isochron follows a curvilinear path that dips toward the spreading center, representing the half-width of the neovolcanic zone. (b) Crustal modeling assuming volcanic construction occurs within an 8-km-wide zone, up to 4 km from the axis. The eruption of lavas over large horizontal distances creates longer isochrons extending farther off-axis. As in Figure 9a, lavas erupted on- or near-axis subside to form the base of the lava pile, steeply rotating toward the spreading center. Lavas emplaced on the surface farther from the axis, as a result of either extensive flow from the axis or eruption off-axis, experience little subsidence, resulting in shallowly dipping isochrons in the upper lavas.

total amount of subsidence determines the orientation of the isochrons while the "width" of the isochrons (the distance that they extend off-axis) represents the approximate half-width of the zone of magmatic construction. If volcanic construction is confined to a narrow, 3-km-wide neovolcanic zone, the resultant isochrons are relatively short (extending ~1.5 km off-axis) and follow curvilinear paths that dip steeply toward the spreading center (Figure 9a). Assuming a significantly wider zone of lava emplacement (up to 4 km from the axis), the isochrons are elongated and dip toward the axis at shallow angles in the upper lavas, which are emplaced up to kilometers from the axis and have experienced little to no subsidence (Figure 9b).

[33] Along the BT scarp, the magnetic isochrons in the lower lava unit dip steeply toward the axis (at angles between 30° and 45° [*Tivey et al.*, 1998]), approximately the same as the dip of the lower lava flows [*Karson et al.*, 2002b], suggesting that these lavas are the product of axial eruptions (Figure 7). In the upper lavas, the isochrons dip at a much shallower angle, suggesting that these lavas were emplaced farther from the axis. Although the magnetic reversal boundary in the upper lavas dips at angles <5°, much shallower than the observed average flow dip of 23.8°, such a discrepancy could result from a difference in scale: the magnetic reversal boundary is less complicated than the actual dips of lava flows, presumably due to the fact that the reversal boundaries are smoothed by the ~1 km transect spacing while individual lava orientations can vary over lateral distances of meters due to irregularities in surface topography or later faulting. While the shallow dip of the magnetic reversal boundary in the upper lavas along the BT appears to suggest a wider zone of accretion than that inferred from the lava orientations, the change in slope of the isochrons also corresponds with the lithologic boundary between the upper (undeformed, shallowly dipping) lavas and lower (deformed, steeply dipping) lavas. Thus the geologic and geophysical evidence support a fundamental distinction between the upper and lower lava units, and suggests that off-axis volcanism (in the form of off-axis eruptions and/or extensive flows emanating from the axis) plays an important role in the accretion of the upper crust on the Cleft Segment.

[34] In this context, the observed difference in composition between the upper and lower lavas along the BT scarp may provide insights into axial and off-axis magmatic construction along the Cleft Segment. In general, the data show a preponderance of relatively primitive compositions among the upper lavas, while the lower lavas tend to be more evolved. This offers further support for the idea that the upper lavas were emplaced by off-axis flows or eruptions that capped the lower lavas

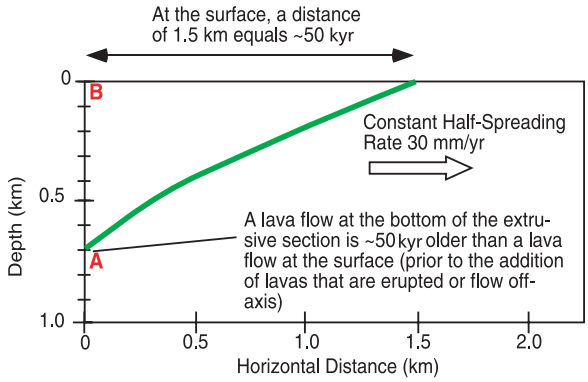

Figure 10. Model isochron (green) for the BT lower lava section based on the thickness of the lower lava unit, the width of the neovolcanic zone, and the dips of lava flows and magnetic isochrons. Prior to the addition of off-axis (upper) lavas, an isochron that intersects the bottom of the lava section (~0.7 km depth) will intersect the surface at a horizontal distance of 1.5 km from the axis (the half-width of the neovolcanic zone [*Kappel and Ryan*, 1986]). At a constant half-spreading rate of 30 km/Myr, 1.5 km represents ~50 kyr. This means that a basalt at the bottom of the extrusive unit along the same isochron (A) is ~50 kyr older than a basalt at the surface (B). The full thickness of the extrusive section is achieved after the capping veneer of upper lavas is erupted or emplaced off-axis later.

accreted on-axis. It should be noted, however, that the compositional difference observed (primitive lavas on top) is opposite to that predicted by Stakes et al. (submitted manuscript, 2005), in which the upper lavas represent off-axis flows that tap the evolved edges of the magma chamber. Alternatively, the compositional distinction may be related to a robust phase of magmatism, during which primitive, voluminous lavas flow off-axis. Once again, our ability to observe robust spatial patterns in the BT lavas may be complicated by our sparse sample coverage and an incomplete understanding of age relations among the lavas. The difficulties we encounter in interpreting temporal evolution and spatial distribution in the BT lavas demonstrate the need for further studies of in situ ocean crust with depth to develop sampling strategies that address variations across both small and large spatial scales.

6.3. Constraints on the Timing of Upper Crustal Accretion

[35] Few investigations have addressed the length of time required to build the various units of oceanic crust. One outgrowth of our examination of the geologic and geophysical evidence for crustal construction is that it can be used to estimate the amount of time it takes to accrete the extrusive section of the crust. The simple calculation that follows is based on the geometry of the dip of the isochrons in the lower lavas, the thickness of the lower section of the extrusive unit, the width of the neovolcanic zone, and the average half-spreading rate. Since the upper lavas may unconformably overlie the lower lavas, and because the isochrons are not well constrained in the upper lavas, we focus our model specifically on the time required to construct the lower lava unit at the spreading axis. The full thickness of the extrusive section is attained some time later, after the addition of off-axis flows.

[36] We used the average dip of lava flows at a given depth in the lower lava unit, which correlates with the dip of the magnetic isochron, to determine the orientation of a model isochron for the BT scarp, shown in Figure 10. The width of the current neovolcanic zone (~3 km [*Kappel and Ryan*, 1986]) and the thickness of the lower lava unit (average ~700 m [*Karson et al.*, 2002b]) were used to constrain the width and height of the model isochron. Immediately following the phase of axial magmatic construction, this model isochron intersects the bottom of the ~0.7 km thick axial (lower) lava unit and would be expressed at the surface over a horizontal distance of 1.5 km, providing that off-axis lavas have not yet been emplaced. Assuming an average half-spreading-rate of 30 mm/yr, simple spreading calculations imply that a horizontal distance of 1.5 km represents 50 kyr. Following the path of the model isochron, a lava flow located at the bottom of the lava pile will be 50 kyr older than a lava flow located vertically above it at the surface. Thus a vertical section through this extrusive unit represents ~50 kyr of accretion, and the thickness of the lava unit accreted at the axis is achieved in this amount of time. The full thickness of the extrusive oceanic crust is achieved sometime later, as a capping veneer of lava is added by off-axis flows and eruptions.

[37] Independent estimates of the length of time required to accrete the extrusive unit are few and, at present, conflicting. One approach, used in a number of seismic studies, is based on the assumption that seismic Layer 2A represents the contact between the extrusive section and the sheeted dike complex; the time it takes to build the extrusive section to its full thickness is then estimated on the basis of the distance off-axis over which Layer 2A thickens [*Christeson et al.*, 1994; *Kent et al.*, 1994;

Vera and Diebold, 1994]. Studies conducted along the super-fast spreading southern EPR (~75 mm/yr half rate) suggest that the extrusive section achieves full thickness (500–600 m) by ~2 km off-axis, or by ~26 kyr [*Kent et al.*, 1994]. For the fast spreading northern EPR (~55 mm/yr half rate), full extrusive thickness (~300 m) is achieved by ~3 km off-axis, or by ~55 kyr [*Vera and Diebold*, 1994]. Adjusting for the difference in spreading rate between the northern and southern EPR and the intermediate spreading Cleft Segment (~30 mm/yr half rate), these studies predict that accretion occurs over ~65 kyr to ~100 kyr on intermediate-spreading ridges. This time period is longer than our estimate based on the isochron model, but may be reasonable when we consider that the full thickness of upper oceanic crust is attained at some distance away from the spreading ridge due to off-axis accretion.

[38] It should be noted that the assumption that Layer 2A represents the base of the extrusive section is controversial, and particularly so with respect to the seismic and geologic data for the Cleft Segment. Canales et al. (submitted manuscript, 2005), for example, showed that Layer 2A thickens to only ~600 m at the Cleft Segment within a few kilometers of the axis, while observations within the BT reveal an extrusive section that is almost double that thickness. In addition, a recent seismic survey on the crust adjacent to the BT suggests that Layer 2A is located within the lava unit, above the intrusive-extrusive boundary (G. Christeson, personal communication). These complications make it difficult to use the Cleft Segment seismic data to independently evaluate our estimate for the timing of accretion.

7. Conclusions

[39] The tectonic window exposed along the BT scarp provides an invaluable opportunity to explore crustal accretion and evolution. Our study reveals that off-axis magmatic construction likely plays an important role in accreting the upper layer of lavas that cap the axial extrusive sequence, supporting a mechanism of crustal thickening based on geological and geophysical investigations. The wide range in lava compositions exposed along the BT scarp also suggests that sampling surface lavas along flow lines may not truly represent changing sub-axial magmatic conditions over time. It is apparent, however, that compelling questions about crustal accretion still remain and will require more detailed sampling and analysis of exposures at the BT and other tectonic windows. Do tectonic windows permit accurate estimates of the time required to build the full thickness of extrusive oceanic crust and how does the timing and architecture of accretion vary with spreading rate? What can be learned about the evolution of axial magmatic processes from samples collected at various depths in the crust both along and perpendicular to isochrons? Clearly there is a need for more detailed sampling within tectonic windows to explore both small- and large-scale variability. This, combined with both radiometric age dating of lavas collected at various depths, and geological and geophysical data should ultimately lead to a comprehensive understanding of the processes of crustal accretion and evolution at mid-ocean ridges.

Acknowledgments

[40] We are grateful to the captain and crew of Atlantis II and WHOI-DSOG. Thoughtful reviews by M. Perfit, S. White, and Associate Editor J. Dixon greatly improved this manuscript. We thank H. Schouten, J. Canales, and G. Christeson for their useful discussions. We appreciate the help of G. Dwyer and M. Rudnicki with the analyses. We also thank M. Perfit, S. Tierney, and D. Naidoo for sharing their work on nearby samples. This work was supported by the US National Science Foundation (OCE 02-22154 to E. K. and J. K. and OCE 9400623 to M. T.).

References

Alt, J. C. (1993), Low-temperature alteration of basalts from the Hawaiian Arch, Leg 136, *Proc. Ocean Drill. Program Sci. Results*, *136*, 133–146.

Alt, J. C., H. Kinoshita, L. B. Stokking, and P. J. Michael (Eds.) (1996), *Proceedings of the Ocean Drilling Program, Scientific Results*, vol. 148, 512 pp., Ocean Drill. Program, College Station, Tex.

Batiza, R., Y. Niu, J. L. Karsten, W. Boger, E. Potts, L. Norby, and R. Butler (1996), Steady and non-steady state magma chambers below the East Pacific Rise, *Geophys. Res. Lett.*, *23*, 221–224.

Bedard, J. H. (1994), A procedure for calculating the equilibrium distribution of trace elements among the minerals of cumulate rocks, and the concentration of trace elements in the coexisting liquids, *Chem. Geol.*, *118*, 143–153.

Byerly, G. (1980), The nature of differentiation trends in some volcanic rocks from the Galapagos spreading center, *J. Geophys. Res.*, *85*, 3797–3810.

Cheatham, M., W. F. Sangrey, and W. M. White (1993), Sources of error in external calibration ICP-MS analysis of geological samples and improved nonlinear drift correction procedure, *Spectrochim. Acta*, *48B*, E487–E506.

Christeson, G. L., G. M. Purdy, and G. J. Fryer (1994), Seismic constraints on shallow crustal emplacement processes at the fast spreading East Pacific Rise, *J. Geophys. Res.*, *99*, 17,957–17,974.

Cotsonika, L. A., M. R. Perfit, D. S. Stakes, and W. I. Ridley (2005), The occurrence and origin of andesites and dacites

from the southern Juan de Fuca Ridge, *Eos Trans. AGU*, *86*(18), Jt. Assem. Suppl., Abstract V13A-04.

Delaney, J. F., F. N. Spiess, W. E. Colony, J. L. Karsten, D. E. Kelley, and P. Nehlig (1987), A complete deep-tow swath map of south-facing "wall" of the Blanco Trough, Juan de Fuca Region, *Eos Trans. AGU*, *68*, 1402.

Delaney, J. R., H. P. Johnson, and J. L. Karsten (1981), The Juan de Fuca Ridge hot spot propagating rift system: New tectonic, geochemical, and magnetic data, *J. Geophys. Res.*, *86*, 11,747–11,750.

Dewey, J. F., and J. M. Bird (1971), The origin and emplacement of the ophiolite suite: Appalachian ophiolites in Newfoundland, *J. Geophys. Res.*, *76*, 3179–3180.

Dilek, Y., E. Moores, D. Elthon, and A. Nicolas (Eds.) (2000), Ophiolites and oceanic crust: New insights from field studies and the ocean drilling program, *Spec. Pap. Geol. Soc. Am.*, *349*, 552 pp.

Dixon, J. E., D. A. Clague, and J.-P. Eissen (1986), Gabbroic xenoliths and host ferrobasalt from the southern Juan de Fuca Ridge, *J. Geophys. Res.*, *91*, 3795–3820.

Embley, R. W., and D. S. Wilson (1992), Morphology of the Blanco transform fault zone N-E Pacific: Implication for it tectonic evolution, *Mar. Geophys. Res.*, *14*, 25–45.

Fornari, D. J., M. R. Perfit, A. Malahoff, and R. Embley (1983), Geochemical studies of abyssal lavas recovered by DSRV Alvin from Eastern Galapagos Rift, Inca Transform, and Ecuador Rift: 1. Major element variations in natural glasses and spatial distribution of lavas, *J. Geophys. Res.*, *88*, 10,519–10,529.

Gast, P. W. (1968), Trace element fractionation and the origin of tholeiitic and alkaline magma types, *Geochim. Cosmochim. Acta*, *32*, 1057–1068.

Goldstein, S. J., M. R. Perfit, R. Batiza, D. J. Fornari, and M. T. Murrell (1994), Off-axis volcanism at the East Pacific Rise detected by uranium-series dating of basalts, *Nature*, *367*, 157–159.

Hawkins, J. W. (2003), Geology of supra-subduction zones–Implications for the origin of ophiolites, in *Ophiolite Concept and the Evolution of Geological Thought*, edited by Y. Dilek and S. Newcomb, *Spec. Pap. Geol. Soc. Am.*, *373*, 227–268.

Hess, P. C. (1989), *Origins of Igneous Rocks*, 336 pp., Harvard Univ. Press, Cambridge, Mass.

Hooft, E. E., H. Schouten, and R. S. Detrick (1996), Constraining crustal emplacement processes from the variation in seismic layer 2A thickness at the East Pacific Rise, *Earth Planet. Sci. Lett.*, *142*, 289–310.

Juteau, T., D. Bideau, O. Dauteuil, G. Manach, D. D. Naidoo, P. Nehlig, H. Ondreas, M. A. Tivey, K. X. Whipple, and J. R. Delaney (1995), A submersible study in the Western Blanco Fracture Zone, N. E. Pacific: Structure and evolution during the last 1.6 Ma, *Mar. Geophys. Res.*, *17*, 399–430.

Kappel, E. S., and W. B. F. Ryan (1986), Volcanic episodicity and a non-steady state rift valley along northeast spreading centers: Evidence from Sea MARC I, *J. Geophys. Res.*, *91*, 13,925–13,940.

Karson, J. A. (1998), Internal structure of oceanic lithosphere: A perspective from tectonic windows, in *Faulting and Magmatism at Mid-Ocean Ridges*, *Geophys. Monogr. Ser.*, vol. 106, edited by W. R. Buck et al., pp. 27–58, AGU, Washington, D. C.

Karson, J. A., E. M. Klein, S. D. Hurst, C. E. Lee, P. A. Rivizzigno, D. Curewitz, A. R. Morris, and Hess Deep '99 Scientific Party (2002a), Structure of uppermost fast-spread oceanic crust exposed near Hess Deep, *Geology*, *20*, 685–688.

Karson, J. A., M. A. Tivey, and J. R. Delaney (2002b), Internal structure of uppermost oceanic crust along the Western Blanco Transform Scarp: Implications for subaxial accretion and deformation at the Juan de Fuca Ridge, *J. Geophys. Res.*, *107*(B9), 2181, doi:10.1029/2000JB000051.

Kent, G. M., A. J. Harding, J. A. Orcutt, R. S. Detrick, J. C. Mutter, and P. Buhl (1994), Uniform accretion of oceanic crust south of the Garrett transform at 14°15′S on the East Pacific Rise, *J. Geophys. Res.*, *99*, 9097–9116.

Klein, E. M., and C. H. Langmuir (1987), Global correlations of ocean ridge basalt chemistry with axial depth and crustal thickness, *J. Geophys. Res.*, *92*, 8089–8115.

Klein, E. M., C. H. Langmuir, and H. Staudigel (1991), Geochemistry of basalts from the Southeast Indian Ridge, 115°E–138°E, *J. Geophys. Res.*, *96*, 2089–2107.

Langmuir, C. H. (1989), Geochemical consequences of in situ crystallization, *Nature*, *420*, 199–205.

Minster, J. F., and C. J. Allegre (1978), Systematic use of trace elements in igneous processes part III: Inverse problem of batch partial melting in volcanic suites, *Contrib. Mineral. Petrol.*, *68*, 37–52.

Moores, E. M., and F. J. Vine (1971), The Troodos massif, Cyprus, and other ophiolites as oceanic crust: Evaluation and implications, *Philos. Trans. R. Soc. London, Ser. A*, *268*, 443–466.

Naidoo, D. D. (1998), Accretion of the upper oceanic crust, Ph.D. dissertation, Univ. of Washington, Seattle.

Nicolas, A. (1989), *Structure of Ophiolites and Dynamics of Oceanic Lithosphere*, 367 pp., Springer, New York.

Pallister, J. S., and C. A. Hopson (1981), Samail ophiolite plutonic suite: Field relations, phase variation and layering and a model of a spreading magma chamber, *J. Geophys. Res.*, *86*, 2593–2644.

Pariso, J. E., and H. P. Johnson (1989), Magnetic properties and oxide petrography of the sheeted dike complex in Hole 504B, *Proc. Ocean Drill. Program Sci. Results*, *111*, 159–166.

Perfit, M. R., and W. W. Chadwick (1998), Magmatism at mid-ocean ridges: Constraints from volcanological and geochemical investigations, in *Faulting and Magmatism at Mid-Ocean Ridges*, *Geophys. Monogr. Ser.*, vol. 106, edited by W. R. Buck et al., pp. 59–116, AGU, Washington, D. C.

Perfit, M. R., D. J. Fornari, A. Malahoff, and R. W. Embley (1983), Geochemical studies of abyssal lavas recovered by DSRV *Alvin* from eastern Galapagos Rift, Inca Transform, and Ecuador Rift: 3. Trace element abundances and petrogenesis, *J. Geophys. Res.*, *88*, 10,551–10,572.

Perfit, M. R., D. J. Fornari, M. C. Smith, J. F. Bender, C. H. Langmuir, and R. M. Haymon (1994), Small-scale spatial and temporal variations in mid-ocean ridge crest magmatic processes, *Geology*, *22*, 375–379.

Regelous, M., Y. Niu, J. I. Wendt, R. Batiza, A. Greig, and K. D. Collerson (1999), Variations in the geochemistry of magmatism on the East Pacific Rise at 10°30′N since 800 ka, *Earth Planet. Sci. Lett.*, *168*, 45–63.

Reynolds, J. F., and C. H. Langmuir (1997), Petrological systematics of the Mid-Atlantic Ridge south of Kane: Implications for ocean crust formation, *J. Geophys. Res.*, *102*, 14,915–14,946.

Reynolds, J. F., C. H. Langmuir, J. F. Bender, K. A. Kastens, and W. B. F. Ryan (1992), Spatial and temporal variability in the geochemistry of basalts from the East Pacific Rise, *Nature*, *359*, 493–499.

Riddihough, R. P. (1984), Recent movement of the Juan de Fuca plate system, *Nature*, *284*, 6980–6995.

Schouten, H., M. A. Tivey, D. J. Fornari, and J. R. Cochran (1999), Central anomaly magnetization high: Constraints on the volcanic construction and architecture of seismic layer 2A at a fast spreading mid-ocean ridge, the EPR at 9°30′–50′N, *Earth Planet. Sci. Lett.*, *169*, 37–50.

Shaw, D. M. (1970), Trace element fractionation during anatexis, *Geochim. Cosmochim. Acta*, *34*, 237–243.

Sinton, J., E. Bergmanis, K. Rubin, R. Batiza, T. K. P. Gregg, K. Grönvold, K. C. Macdonald, and S. M. White (2002), Volcanic eruptions on mid-ocean ridges: New evidence from the superfast spreading East Pacific Rise, 17°–19°S, *J. Geophys. Res.*, *107*(B6), 2115, doi:10.1029/2000JB000090.

Sinton, J. M., D. S. Wilson, D. M. Christie, R. N. Hey, and J. R. Delaney (1983), Petrologic consequences of rift propagation on oceanic spreading ridges, *Earth Planet. Sci. Lett.*, *62*, 193–207.

Smith, M. C., M. R. Perfit, and I. R. Jonasson (1994), Petrology and geochemistry of basalts from the southern Juan de Fuca Ridge: Controls on the spatial and temporal evolution of mid-ocean ridge basalt, *J. Geophys. Res.*, *99*, 4787–4812.

Soule, S. A., D. J. Fornari, M. R. Perfit, M. A. Tivey, W. I. Ridley, and H. Schouten (2005), Channelized lava flows at the East Pacific Rise crest 9°–10°N: The importance of off-axis lava transport in developing the architecture of young oceanic crust, *Geochem. Geophys. Geosyst.*, *6*, Q08005, doi:10.1029/2005GC000912.

Stewart, M. A., E. M. Klein, and J. A. Karson (2002), Geochemistry of dikes and lavas from the north wall of the Hess Deep Rift: Insights into the four-dimensional character of crustal construction at fast spreading mid-ocean ridges, *J. Geophys. Res.*, *107*(B10), 2238, doi:10.1029/2001JB000545.

Stewart, M. A., E. M. Klein, J. A. Karson, and J. G. Brophy (2003), Geochemical relationships between dikes and lavas at the Hess Deep Rift: Implications for magma eruptibility, *J. Geophys. Res.*, *108*(B4), 2184, doi:10.1029/2001JB001622.

Sun, S.-S., and W. F. McDonough (1989), Chemical and isotopic systematics of oceanic basalts: Implications for mantle composition and process, in *Magmatism in the Ocean Basins*, edited by A. D. Saunder and M. J. Norry, *Geol. Soc. Spec. Publ.*, *42*, 3313–3345.

Tierney, S. E. (2003), Distribution and composition of lavas from the southern Cleft Segment of the Juan de Fuca Ridge: Tectonomagmatic evolution of a ridge-transform intersection, Masters thesis, Univ. of Florida, Gainesville.

Tivey, M. A. (1996), Vertical magnetic structure of ocean crust determined from near-bottom magnetic field measurements, *J. Geophys. Res.*, *101*, 20,275–20,296.

Tivey, M. A., H. P. Johnson, C. Fleutelot, S. Hussenoeder, R. Lawrence, C. Waters, and B. Wooding (1998), Direct measurement of magnetic reversal polarity boundaries in a cross-section of oceanic crust, *Geophys. Res. Lett.*, *25*, 3631–3634.

Vera, E. E., and J. B. Diebold (1994), Seismic imaging of oceanic layer 2A between 9°30′N and 10° on the East Pacific Rise from two-ship wide-aperture profiles, *J. Geophys. Res.*, *99*(B2), 3031–3042.

Weaver, J., and C. H. Langmuir (1990), Calculation of phase equilibrium in mineral-melt systems*Comput. Geosci.*, *16*, 1–19.

Wilson, D. S., R. N. Hey, and C. Nishimura (1984), Propagation as a mechanism of reorientation of the Juan de Fuca Ridge, *J. Geophys. Res.*, *89*, 9215–9225.